Coatings **2014**, *4*, 18-36; doi:10.3390/coatings4010018

OPEN ACCESS

coatings

ISSN 2079-6412

www.mdpi.com/journal/coatings

Article

Abrasion, Erosion and Cavitation Erosion Wear Properties of Thermally Sprayed Alumina Based Coatings

Ville Matikainen *, Kari Niemi, Heli Koivuluoto and Petri Vuoristo

Department of Materials Science, Tampere University of Technology, Korkeakoulunkatu 6, FI-33720 Tampere, Finland; E-Mails: kari.niemi@tut.fi (K.N.); heli.koivuluoto@tut.fi (H.K.); petri.vuoristo@tut.fi (P.V.)

***** Author to whom correspondence should be addressed; E-Mail: ville.matikainen@tut.fi; Tel.: +358-4-0198-1854; Fax: +358-3-3115-2330.

Received: 7 November 2013; in revised form: 2 December 2013 / Accepted: 18 December 2013 / Published: 2 January 2014

Abstract: Thermally-sprayed alumina based materials, e.g., alumina-titania (Al_2O_3-TiO_2), are commonly applied as wear resistant coatings in industrial applications. Properties of the coatings depend on the spray process, powder morphology, and chemical composition of the powder. In this study, wear resistant coatings from Al_2O_3 and Al_2O_3-13TiO_2 powders were sprayed with plasma and high-velocity oxygen-fuel (HVOF) spray processes. Both, fused and crushed, and agglomerated and sintered Al_2O_3-13TiO_2 powders were studied and compared to pure Al_2O_3. The coatings were tested for abrasion, erosion, and cavitation resistances in order to study the effect of the coating structure on the wear behavior. Improved coating properties were achieved when agglomerated and sintered nanostructured Al_2O_3-13TiO_2 powder was used in plasma spraying. Coatings with the highest wear resistance in all tests were produced by HVOF spraying from fused and crushed powders.

Keywords: abrasion; erosion; cavitation; plasma spray; high-velocity oxygen-fuel (HVOF); alumina; alumina-titania

---

1. Introduction

Metal components are the basis of engineering applications and constructions and are exposed to wide range of conditions and environments, e.g., in process industries. The ductile metallic base material can be subjected to different types of wear by the surrounding operation environment. In such cases, hard thermal spray coatings can be utilized to improve the wear resistance of the metallic surface [1]. Alumina (Al_2O_3) and alumina-titania (Al_2O_3-TiO_2) materials are widely used as thermally-sprayed protective coatings against abrasion, erosion, and cavitation erosion wear, e.g., in textile, pulp and paper, and pump industries [2]. Alumina is a hard and relatively cheap material with high hardness, good wear, and corrosion and thermal resistance [2,3]. It has also high electric resistance, which has made Al_2O_3 attractive for coating applications where electric insulation and high breakthrough voltage is sought. Fracture toughness of Al_2O_3 coatings can be increased by small addition of TiO_2, which is mechanically blended with Al_2O_3 particles or mechanically cladded on the Al_2O_3 particles as a layer of small TiO_2 particles [1]. As a down side, the added TiO_2 also decreases hardness and wear resistance of the coating [2]. During the last decade, nanostructured powders have been gaining increasing attention and improved coating properties, e.g., higher toughness, adhesion, and wear resistance, have been reported [4–8]. Typically, Al_2O_3 and Al_2O_3-TiO_2 powders have been manufactured by blending Al_2O_3 and TiO_2 fused and crushed powders or by cladding Al_2O_3 particles with TiO_2. Manufacturing of the nanostructured spherical particles with good flowability is most commonly done by spray drying. The powder manufacturing method and TiO_2 distribution in the powder and sprayed coating has been studied and found to affect the coating properties [8–10]. Evenly distributed TiO_2 in the spray-dried powders improves the coating properties compared to coatings sprayed using blended or mechanically clad powders resulting in distinguishable areas of Al_2O_3 and TiO_2 [8,10].

The Al_2O_3 coatings are typically sprayed with plasma torch, which is capable of melting generally any material with sufficient difference between the material's melting and vaporization (or decomposition) temperature [11]. The particle size distribution of oxide ceramic powders used in conventional plasma spraying is often +45-22 μm. Plasma formation related arc fluctuation and different particle sizes combined with radial powder feeding result in wide range of particle trajectories and thermal histories. This scattering causes defects in the coating structure, e.g., partially molten particles, unmolten particles, and related porosity. One approach to improve the Al_2O_3 coatings has been the use of high-velocity oxygen fuel (HVOF) spray process, which is based on combustion of oxygen and fuel gas or liquid. The melting temperature of Al_2O_3 is 2040 °C, which makes it possible to be sprayed also by combustion based spray processes, e.g., flame spraying and HVOF spraying [12–16]. Maximum flame temperatures between 2828 and 3160 °C can be achieved depending on the used fuel gas [17]. Very dense coatings can be produced by HVOF spray processes compared to plasma-sprayed coatings due to the higher particle velocity. In general, smaller particle size is necessary for sufficient melting of the particles in the HVOF process compared to plasma spraying. The melting and deposition efficiency of HVOF-sprayed ceramics have been regarded as low, but this has been overcome by the use of ethylene as the fuel gas [17]. The requirement for spraying Al_2O_3, and other ceramics, with HVOF processes, is the sufficient particle flight time and heating from the powder injection to the point where the gas jet temperature drops below the particle temperature. This has been achieved by using HVOF torches with the powder injection located in the combustion chamber [2].

Typically, the Al_2O_3 coatings are produced with plasma spraying. During recent years, the coating properties have been improved by the use of HVOF processes, as well as with the development of nanostructured powders for plasma spraying, *i.e.*, agglomerated and sintered powders from nanosized primary particles. Both, nanostructured coatings and HVOF-sprayed coatings have been reported to possess significantly higher wear resistance compared to conventional plasma-sprayed coatings [4–8,18,19]. However, the performance of nanostructured plasma-sprayed coatings and HVOF-sprayed ceramic coatings has not been truly compared under abrasive, erosive, and cavitation erosion wear. The cavitation erosion of thermally-sprayed coatings has been studied increasingly during the last decades, but most of the studies have focused on metallic and carbide coatings [20–23], while ceramic materials, and especially ceramic coatings, have not been studied as actively. Some cavitation erosion studies of bulk ceramics have been published [24–26], but only few studies concerning thermally-sprayed ceramic coatings [27–29]. Typically, these materials have a brittle structure and lower cohesion, which results in considerably lower resistance against cavitation erosion as compared to, e.g., carbide coatings. The coating properties provided by HVOF spraying and nanostructured powder materials, however, are potential candidates to improve the performance of ceramic coatings in cavitation erosion environments.

Alumina-based coatings are applied to various applications, in which they are exposed to different types of wear, e.g., abrasion, erosion, or cavitation erosion wear. Especially, the current research on erosion wear properties of HVOF-sprayed ceramic coatings and cavitation erosion wear of ceramic coatings is very limited. For this reason, it is important to study the wear behavior of ceramic coatings under solid particle erosion and cavitation erosion. By comparing the results to abrasion wear behavior, a good understanding of the overall coating performance can be drawn. In this study, Al_2O_3 and Al_2O_3-$13TiO_2$ powders with different morphologies (agglomerated and sintered *vs.* fused and crushed) were sprayed with atmospheric plasma spray (APS) and high-velocity oxygen fuel (HVOF) spray systems. Structures and the wear behavior of these coatings were studied under abrasion, erosion, and cavitation erosion wear conditions.

2. Experimental Techniques

2.1. Coating Manufacturing

Alumina-based coatings were produced by atmospheric plasma spraying (APS) and high-velocity oxygen-fuel (HVOF) spraying. APS coatings were sprayed with Plasma Technik A-3000S 4/2 plasma spray system equipped with a conventional F4MB (Sulzer Metco AG, Switzerland) plasma torch using a radial powder injection. Argon and hydrogen were used as process gases. HVOF coatings were sprayed with TopGun (GTV Gmbh, Germany) spray gun. A variety of process gasses can be used with TopGun and it has 22 mm long combustion chamber, which makes it especially capable of spraying ceramic powders. Ethylene was used as fuel gas for the HVOF spraying. Spray parameters for APS and HVOF spray processes are presented in Tables 1 and 2, respectively. Coatings were sprayed on grit-blasted (Al_2O_3 grits, 36 Mesh) 20 mm × 100 mm × 5 mm low carbon steel (Fe52) substrates.

Table 1. Spray parameters for plasma spraying (APS).

Spray Parameter	Powder	
	Al_2O_3	Al_2O_3-13TiO_2
Current [A]	600	530
Argon [slpm]	41	41
Hydrogen [slpm]	14	14
Nozzle diameter [mm]	6	6
Spray distance [mm]	120	120
Powder feed rate [g/min]	30	30

Table 2. Spray parameters for high-velocity oxygen fuel (HVOF).

Spray parameter	Powder
	Al_2O_3, Al_2O_3-13TiO_2
Ethylene [slpm]	93
Oxygen [slpm]	270
Spray distance [mm]	150
Chamber/nozzle [mm]	22/135
Powder feed rate [g/min]	40

2.2. Powder Materials

Table 3 shows the information of the powders used in this study. Fused and crushed Al_2O_3 powders were sprayed with APS and HVOF spray processes. Particle sizes were optimized for both processes. Coarser powders were used for plasma spraying and the finer powders for HVOF spraying. In addition, two different powder types of Al_2O_3-13TiO_2 were used in both spray processes (with optimized particle sizes). Al_2O_3-13TiO_2 powders were either fused and crushed or agglomerated and sintered. Agglomerated and sintered powders, having the nanostructures, consist of small evenly distributed primary particles of Al_2O_3 and TiO_2. These powders have spherical powder morphology, which is presented in Figure 1a. The primary particle size after manufacturing process is approximately from 50 to 500 nm, with few larger particles up to 1500 nm. The conventional powders of Al_2O_3 and Al_2O_3-TiO_2 are manufactured by fusing and crushing method, resulting in dense irregular blocky particles. The powder morphology of fused and crushed Al_2O_3-TiO_2 blended powder is presented in Figure 1b. Some lighter grey TiO_2 particles can be observed in Figure 1b, while darker grey particles are Al_2O_3.

Table 3. Information of the used powders and sample names, F/C stands for fused and crushed, and A/S for agglomerated and sintered.

Sample name	Chemical Composition	Manufacturing method	Manufacturer	Trade name	Particle size [µm]	Spray method
APS_A	Al_2O_3	F/C	H.C. Starck, Goslar, Germany	Amperit 740.1	-45+22	Plasma
HVOF_A	Al_2O_3	F/C	H.C. Starck, Goslar, Germany	Amperit 740.8	-20+5	HVOF
APS_AT1	Al_2O_3-13TiO_2	F/C	Sulzer Metco, Wohlen, Switzerland	Amdry 6228	-45+22	Plasma

Table 3. *Cont.*

Sample name	Chemical Composition	Manufacturing method	Manufacturer	Trade name	Particle size [µm]	Spray method
HVOF_AT1	Al_2O_3-13TiO_2	F/C	Sulzer Metco, Wohlen, Switzerland	Amdry 6220	-22+5	HVOF
APS_AT2	Al_2O_3-13TiO_2	A/S	Millidyne, Tampere, Finland	Neoxid A103	-45+9	Plasma
HVOF_AT2	Al_2O_3-13TiO_2	A/S	Millidyne, Tampere, Finland	Neoxid A103	-32+5	HVOF

Figure 1. Powder morphologies of (**a**) agglomerated and sintered Al_2O_3-13TiO_2 powder (Neoxid A103, HVOF cut) and (**b**) fused and crushed Al_2O_3-13TiO_2 powder (Amdry 6228, APS cut). SEM images.

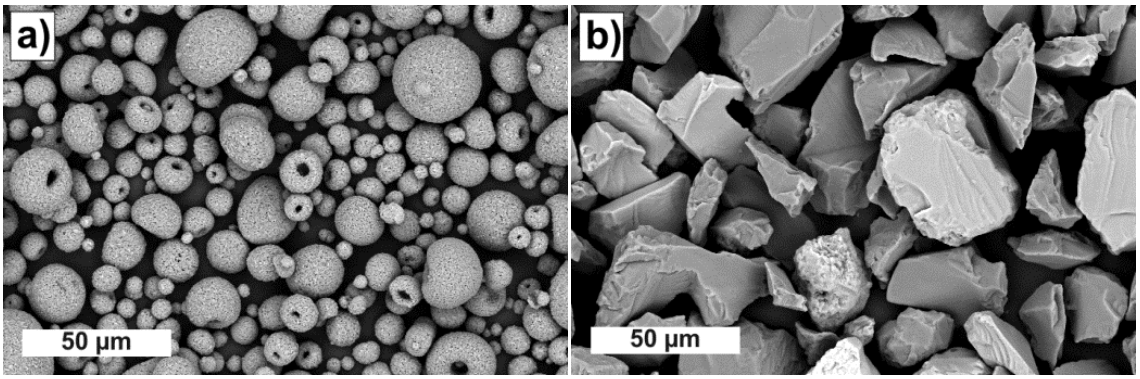

2.3. Characterisation Techniques

Coating microstructures were analyzed using a field-emission scanning electron microscope (FE-SEM), (ULTRAplus, Carl Zeiss Microscopy GmbH, Germany). Structures were studied from metallographic cross-sectional coating samples. General coating structures, powder morphologies, and worn surfaces after wear tests were characterized with a scanning electron microscope, SEM (XL30, Philips, The Netherlands). Furthermore, mechanical behavior of the coatings was investigated by microhardness measurements. Vickers hardnesses (HV0.3) were measured as an average of 10 measurements using a microhardness tester (MMT-X7, Matsuzawa, Japan).

2.4. Wear Tests

Abrasion wear behavior of the coatings was evaluated using a modified version of the ASTM G 65 dry rubber-wheel abrasion test, where five samples could be tested simultaneously. The total duration of the test was 60 min. Weight losses were measured after each 12-minute period with an accuracy of 0.001 g. The surface speed of the rubber wheel was 1.64 m/s, which resulted in a total wear length of 5900 m. Each sample was pressed against the rubber wheel with a force of 13 N. The test simulates three-body abrasion condition, where dry quartz sand (SiO_2) with a grain size of 0.1–0.6 mm was used as an abrasive (Figure 2). The flow rate of the abrasive was 25 g/min. The results are given as an average of three measurements. The sample surfaces were fine-grinded (1200 SiC paper) to remove the surface roughness of the as-sprayed coatings.

Figure 2. SEM image of the quartz sand used in abrasion and erosion wear tests.

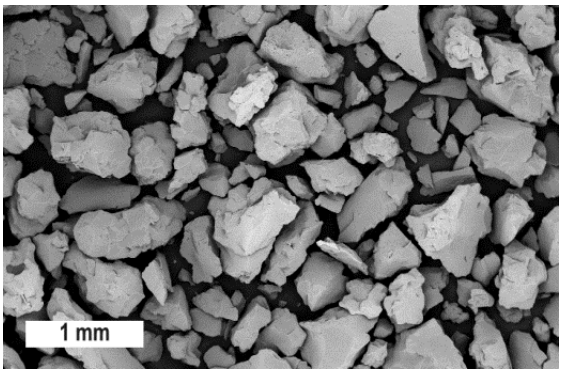

Erosion wear behavior of the coatings was studied with a centrifugal erosion tester. Total amount of 12 samples were attached simultaneously in the sample holders, located on the outer ring in fixed positions. Sample holders, with angles of 30 and 90 degrees, were used. Rotation speed was set to 6000 rpm for the test and 1 kg of the same quartz sand as in abrasion wear test was used as the erosive. The sample surfaces were fine-grinded (1200 SiC paper) before tests.

Cavitation erosion tests were performed with an ultrasonic transducer (VCX-750, Sonics & Materials, USA) according to the ASTM G32-10 standard [30]. The optional stationary specimen method described in the standard was used. Schematic presentation of the test setup is shown in Figure 3a. The coating surfaces to be tested were grinded flat and polished with a polishing cloth and diamond suspension (3 μm). Samples were cleaned in ultrasonic bath with ethanol and weighed after drying. Samples were attached on a stationary sample holder and the head of the ultrasonic transducer was placed at the distance of 0.5 mm. Samples were weighed after 5, 15, 30, 60, 90, and 120 min. Depending on the wear rate, samples were tested further for a total of 150 or 210 min. A replaceable tip made of Ti-6Al-4V was used as the cavitation resistant horn piece (Figure 3b).

Figure 3. Cavitation erosion test (**a**) schematic presentation of test setup, modified from ASTM G32-10 standard [29] and (**b**) the replaceable Ti-6Al-4V tip used.

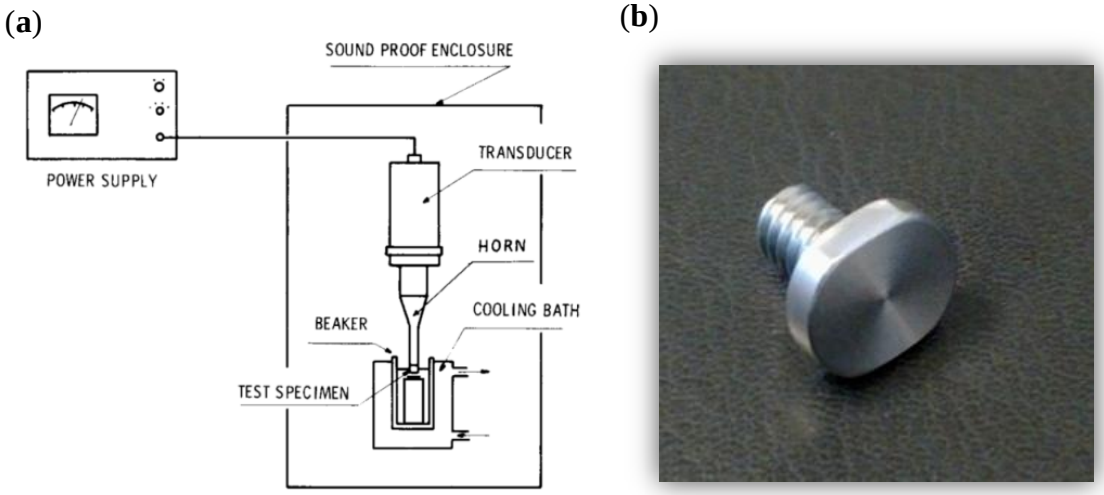

3. Results and Discussion

3.1. Coating Microstructure

The cross-sections of the coatings were studied with FE-SEM. General views of the coating structures are presented in Figure 4 (APS coatings in 4a–c and HVOF coatings in 4d–f). All coatings are relatively dense. In addition, all HVOF-sprayed coatings were denser compared to their plasma counterparts. The coatings sprayed from fused and crushed powders showed typical coating structure with evenly distributed porosity. The HVOF_AT2 coating showed more large pores compared to other HVOF coatings. The porosity was found to result from pull-outs and removal of completely unmelted particles in the structure.

Figure 4. Structure of (**a**) APS_A; (**b**) APS_AT1 (F/C); (**c**) APS_AT2 (A/S); (**d**) HVOF_A; (**e**) HVOF_AT1 (F/C); and (**f**) HVOF_AT2 (A/S) coatings. SEM images.

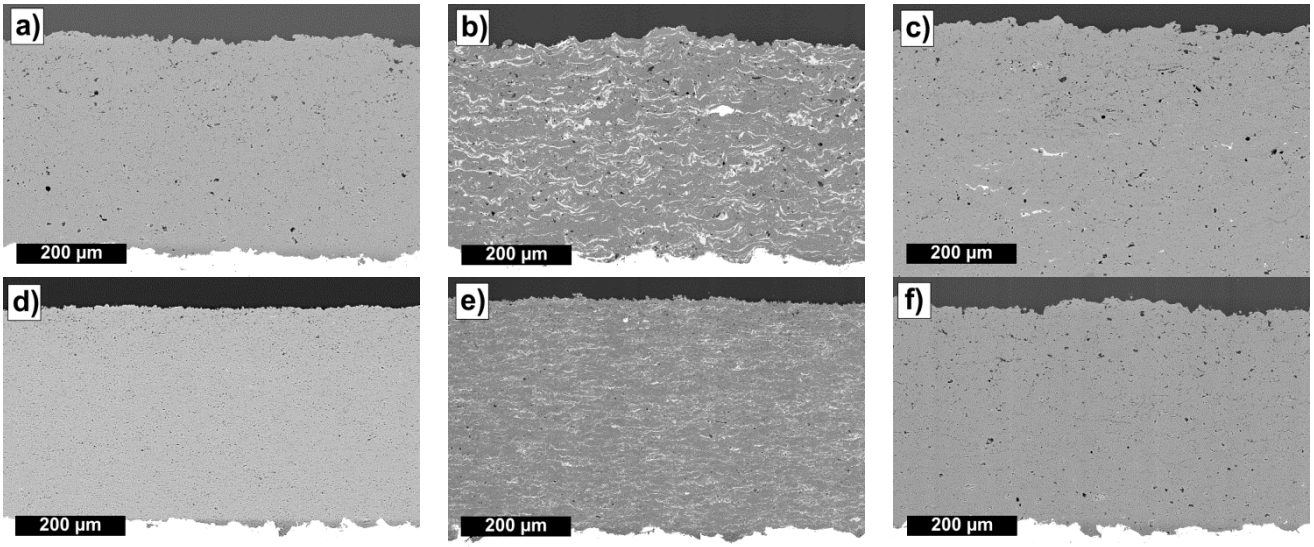

The detailed microstructures of APS_A and APS_AT1 (F/C) coatings are presented in Figure 5. Both coatings show a quite distinctive vertical microcracking of the lamellas throughout the coating resulting from locally insufficient bonding and relaxation of quenching stresses [31]. The thickness of the white TiO_2 lamellas in the coating sprayed from the blended powder ranges from submicron thickness to a few micrometers (Figure 5b). The adherence of the TiO_2 lamellas in the structure seems to be good and there is no observable cracking particularly related to TiO_2 splats.

Figure 5. Microstructure of (**a**) APS_A and (**b**) APS_AT1 coatings. FE-SEM images.

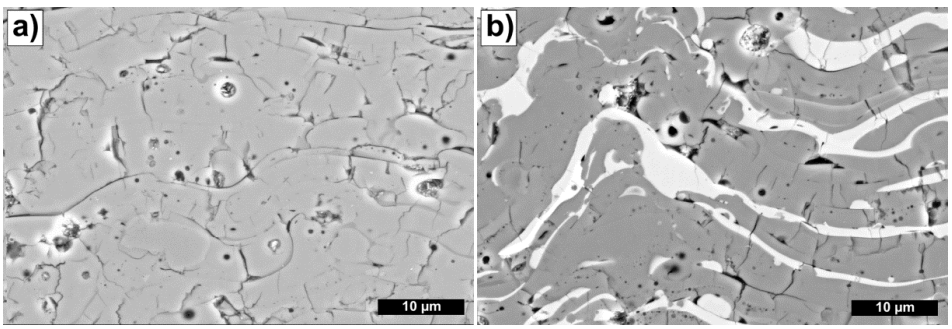

Very dense HVOF coatings were produced from the fused and crushed powders. Both HVOF_A (Figure 6a) and HVOF_AT1 (Figure 6b) coatings have a few visible, insufficiently melted, rounded Al_2O_3 particles in the structure. The TiO_2 particles in Figure 6b seem to have melted completely during the spray process. Both coatings show some vertical cracking, but limited cracking of splat interfaces as compared to plasma-sprayed coatings. Structural details of all HVOF-sprayed coatings were smaller compared to APS coatings due to the smaller particle size distribution used. In addition, the higher velocity involved in the HVOF process promoted the more complete filling of the surface roughness during the spraying. This can be seen from the filling of the surface around the partially melted Al_2O_3 particles in both coatings. It can be speculated if the smaller size of the particles also leads to lower quenching stresses as a result of smaller flattened particle size and larger number of splats sharing the stresses forming in the coating. The smaller diameter of the splat would mean smaller quenching stresses if full contact and good adhesion between flattened particle and surface is expected. In addition, the high velocity impact of the small Al_2O_3 particles have been reported reaching extremely high cooling rates, which can promote the formation of nanocrystalline γ-Al_2O_3 phase or even an amorphous structure [32]. Furthermore, Sakoda *et al.* [33] have reported that the hardness values of different structures in Al_2O_3 coatings vary between α-Al_2O_3, γ-Al_2O_3 and nanocrystalline phases.

Figure 6. Microstructure of (**a**) HVOF_A and (**b**) HVOF_AT1 coatings. FE-SEM images.

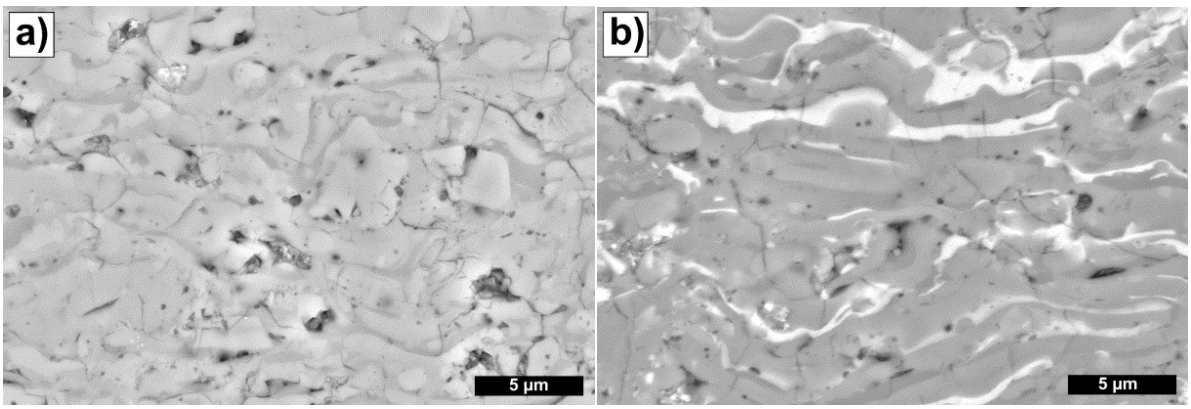

When comparing the structures of APS- and HVOF-sprayed coatings from agglomerated and sintered Al_2O_3-13TiO_2 powders (APS_AT2 and HVOF_AT2), they showed unique structure with partially molten composite particles. A partially molten particle from APS_AT2 coating is visible in Figure 7a and it consists of lighter and darker grey areas. The color difference arises from the variation of TiO_2 content within the partially molten particle. TiO_2 melts at lower temperature (1854 ℃) than pure Al_2O_3 (2040 ℃) [7] and has been suggested of existing as solid solution with γ-Al_2O_3 [9]. The lighter segregated areas were found to contain more TiO_2 than the darker areas, based on EDS analysis. This sort of partially molten structure has higher viscosity than fully molten particles, which presents a risk of increased coating porosity during plasma spraying. These particles are not able to flatten as well as fully molten particles, which can lead to insufficient filling of surface roughness. Similar composite structures exist in the HVOF-sprayed coating in Figure 7b. It is noteworthy that the flattening and bonding of the partially molten areas seems better compared to APS-sprayed coating, *i.e.*, lamella interfaces are less visible. Despite the dense structure, regions of completely unmolten particles were also found in the detailed structural characterization of the HVOF_AT2 coating. These particles showed clearly the loose

structure of the powder primary particles. The reason for the existence of unmolten particles in the coating is most likely caused by the large particles that do not even have the sufficient time to be partially melted from the inside. The surface of such particle starts melting during the spray process, but the melt front does not have the time to reach the insides of the particle. In addition, porosity inside the agglomerated and sintered particle can slow down the melting [34].

Figure 7. Structural details: (**a**) Partially molten area in APS_AT2 coating; and (**b**) partially molten and unmolten areas in the HVOF_AT2 coating. FE-SEM images.

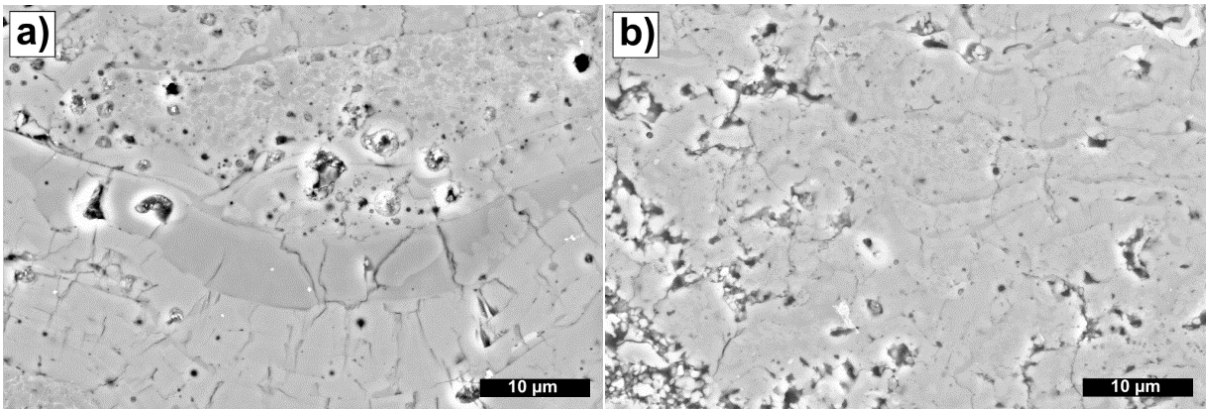

3.2. Hardness Measurements

The Vickers hardness values (HV0.3) of the coatings are displayed in Table 4. Both coatings sprayed from the agglomerated and sintered powders show slightly lower hardness values compared to the coatings sprayed from fused and crushed powders. There was not any significant difference in the hardness values between the Al_2O_3 and Al_2O_3-TiO_2 coatings sprayed from fused and crushed powders.

Table 4. Vickers hardness values (HV0.3) and standard deviations of the coatings.

Measured quantity	APS_A	HVOF_A	APS_AT1	HVOF_AT1	APS_AT2	HVOF_AT2
Hardness [HV0.3]	1105	1117	1089	1075	1009	1027
Standard deviation	171	54	102	58	142	81

3.3. Cavitation Erosion Wear Resistance

Laboratory scale accelerated test carried out with an ultrasonic transducer is a fast way of testing the material's resistance to cavitation erosion [30]. The tests ability to mimic most real application conditions can be argued, but it provides standard conditions where the materials erosion resistance to bubble collapse induced shocks, i.e., cavitation erosion, can be tested. Indeed, the test can be thought as if the coating surface was continuously bombarded by shock waves produced by the numerous cavitation bubbles collapsing near the sample surface. The bubble size without the sample surface can be expected to be approximately 10 µm [35].

The graph in Figure 8 shows the weight losses of the samples as a function of time. It can be noticed that all the samples have linear weight loss, i.e., constant wear rate, throughout the test. For bulk metallic samples, the cavitation erosion wear rate curve typically includes an incubation period in the beginning,

during which the metal surface is plastically deformed and no weight loss is observed. After this acceleration stage takes place and the wear rate of the metallic sample starts increasing [36]. This, however, is not the case with brittle ceramic coatings. Incubation stage cannot be observed as wear begins immediately by the removal of the poorly adhered particles from the surface. In addition, the acceleration phase of ceramic coatings seems to take place during the very first minute. This difference between sprayed coatings and bulk materials was also noted by Schwetzke and Kreye [28] in their study of HVOF coatings. The linear wear rates of the samples observed in the graph indicate that the maximum wear rate is reached during the very first minutes.

Figure 8. Weight losses of APS and HVOF coatings and Ti-6Al-4V tip material *versus* time in the cavitation erosion test.

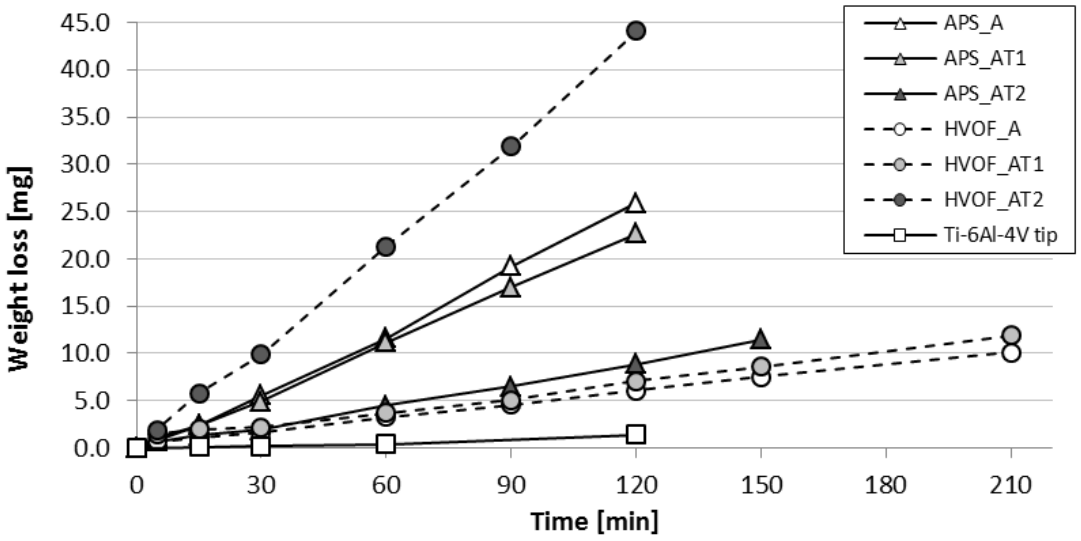

The highest cavitation erosion resistance was observed on the coatings HVOF_A, HVOF_AT1 and APS_AT2 with 3.0, 3.4 and 4.6 mg/h wear rate, respectively. Both, APS_A and APS_AT1, plasma-sprayed coatings eroded faster with wear rates of 13.0 and 11.4 mg/h. The highest wear rate was measured for HVOF_AT2 coating (22.1 mg/h). The very good performance of APS_AT2 coating was due to improved coating cohesion by the evenly distributed TiO_2 in the powder and coating. Overall, the cavitation erosion test gives very good information about the coating structure and cohesion as the coating defects are the major factors accelerating the erosion.

The heterogeneous structure of the thermally-sprayed oxide coating consists of (1) well melted structure, (2) partially or unmelted particles, (3) lamella interfaces, (4) porosity, and (5) microcracks [37]. The reason for observed linear wear behavior of all the coating samples derives from the coating structure and material properties. As cavitation erosion begins, the shock waves created by the collapse of the cavitation bubbles near the surface start working the whole surface area. Poorly bonded particles or lamellas on the polished surfaces are the first ones to be removed by the cavitation erosion. Simultaneously, the well-melted areas of the coating surface start undergoing cavitation erosion. Typically, good cavitation erosion resistance is linked to material ductility and cohesion [36], which could favor the composite structures and evenly distributed TiO_2 observed in the coatings produced from agglomerated and sintered powders.

Single lamella in the coating consists of microcracks as shown in Figure 9a. These microcracks are caused by the quenching stresses during the cooling of the lamella. The weak areas mostly worked by the cavitation erosion are the visible edges of the lamella as well as the microcrack network. The wear mechanism of single lamella can be seen in Figure 9b and the material removal seems to take place purely by brittle fracture. The coating's characteristic columnar structure is being picked apart, especially from the edges and the microcracks. A closer image of material loss from the microcracks is presented in Figure 9c. The arrow points to a small particle about to be fractured and removed at the intersection of microcracks. When the microcracks of the lamella have propagated and connected with other cracks, larger pieces are removed. This is further promoted by the fact that the lamellas of plasma-sprayed coating are only partially in contact with the underlying surface. As the erosion wear progresses, the surface becomes rougher and takes a more blocky form. The small-scale erosion of the lamella is not, however, the main mechanism of material removal. Major fraction of the coating removal takes place in larger particles and the controlling factor of the erosion rate is the overall strength of the coating and the amount of defects, e.g., splat interfaces. Most of the material is lost in larger blocky particles, as a result of crack propagation through quenching cracks and poor interfaces. This mechanism typically involves several splats simultaneously. The debris particle size is smaller for coatings with good cohesion and small-scale structure, e.g., HVOF-sprayed coatings from fused and crushed powders, whereas very large debris particles can be observed for coatings with large amounts of poorly melted particles and low cohesion. Some debris from the agglomerated and sintered coating of Al_2O_3-13TiO_2 (APS_AT2), containing partially molten particles, is presented in Figure 10a. The rough surface of the particle shows the partially molten structure. The structure consists of Al_2O_3 regions in TiO_2-rich matrix. Similar structure from the cross section sample was presented in Figure 7a, showing the same granular texture. A debris particle from a well-melted region of the same coating is presented in Figure 10b. The debris particle shows blocky surface of a brittle fracture and the columnar structure of the lamellas is visible. The top and bottom sides of the particle show larger areas of smooth splat surface. When the cohesion of the coating is poor and the structure includes large amounts of weak surfaces, e.g., splat interfaces, the debris particle size and shape change drastically from the well-melted particle seen in Figure 10b. The HVOF_AT2 coating showed poor performance in cavitation erosion tests and debris particle from the coating can be seen in Figure 10c. The size of the particle is large, approximately 60–100 μm, and the shape is rough but not blocky as would be the case if cracking through splats took place. The failure has progressed through the weak boundaries of insufficiently melted particles.

When comparing APS- and HVOF-sprayed coatings and their wear surfaces, the wear mechanism seemed to be the same. As the particle size for HVOF-sprayed ceramic coatings are significantly smaller, also the lamellae size and thickness are smaller. This leads to smaller structural details of the coatings, as well as the wear surface. Another significant difference between plasma- and HVOF-sprayed coatings from fused and crushed powders, is the size of the horizontal cracks existing between splats. Better bonding of HVOF coatings promotes the good cavitation erosion resistance.

Figure 9. (**a**) Lamella on as-sprayed APS_A coating; (**b**) Lamella after cavitation erosion (APS_A); (**c**) Microcracks being worked at by cavitation erosion (APS_A).

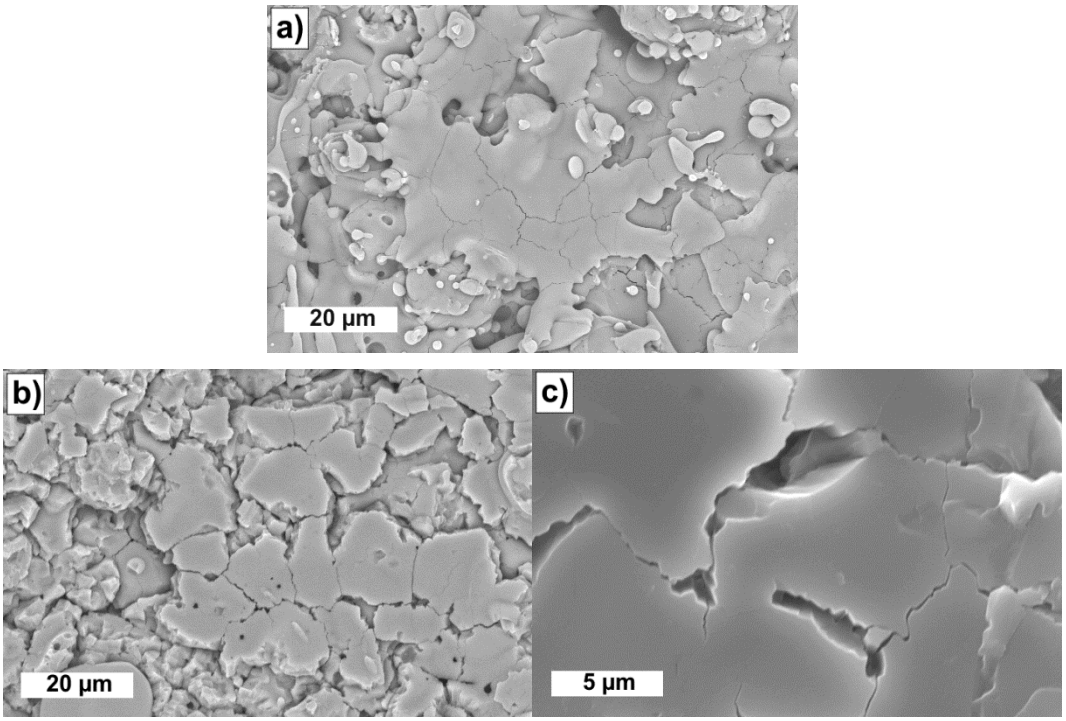

Figure 10. (**a**) Partially molten agglomerated and sintered Al_2O_3-13TiO_2 particle removed during cavitation erosion test (APS_AT2); (**b**) Well-melted region of the same coating removed during cavitation erosion test (APS_AT2); (**c**) Large debris particle from HVOF_AT2 coating.

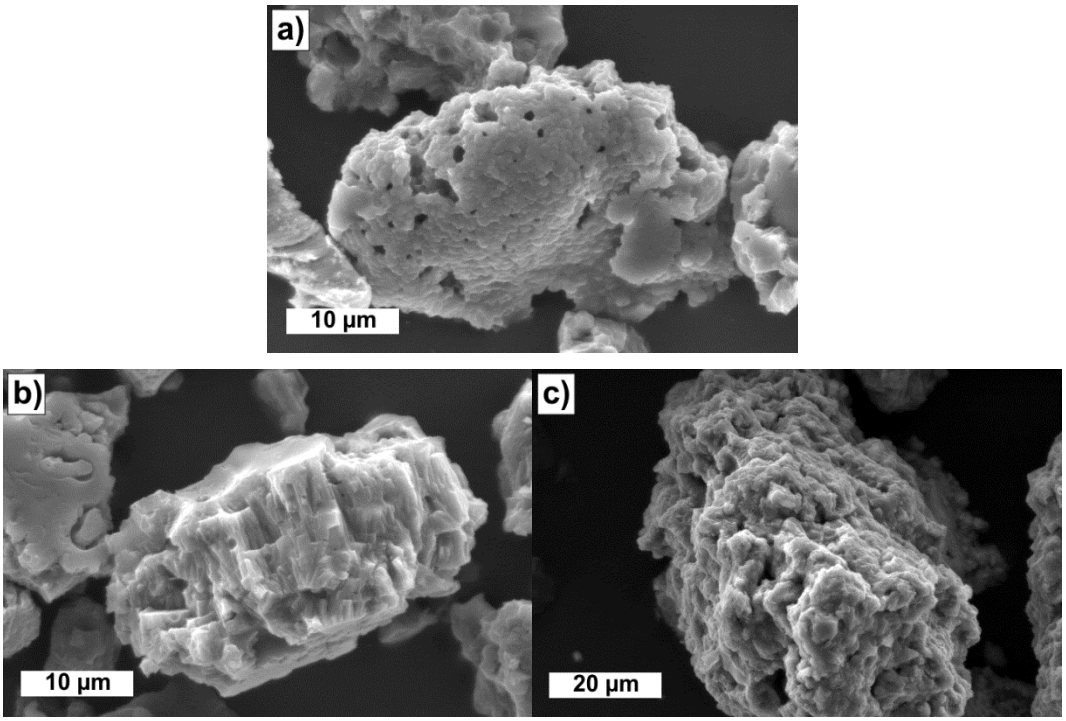

3.4. Abrasion Wear Resistance

HVOF-sprayed ceramic coatings have generally been reported as having better mechanical properties and higher abrasion resistance [18,19] compared to their conventionally plasma-sprayed counterparts. The better performance is due to the smaller particle size and higher particle velocity during the spraying. These features of HVOF-sprayed ceramic coatings make it possible to produce dense coatings with fine microstructure. The weight losses after the rubber wheel dry-abrasion tests are shown in Figure 11. The high-abrasion-wear resistance of HVOF coatings sprayed from fused and crushed powders (HVOF A and HVOF_AT1) is clearly detected. Indeed, the performance of HVOF coatings was comparable with bulk Al_2O_3. Coatings sprayed from the agglomerated and sintered powders, on the other hand, did not rank in the same way, as the plasma-sprayed APS_AT2 coating performed better (86 mg) than the HVOF sprayed HVOF_AT2 coating (116 mg). Even though the HVOF sprayed coating seemed to be very dense in Figure 4f, the coating structure was found to contain more unmelted particles compared to the APS coating. This decreases the abrasion resistance in dry-abrasion rubber wheel test due to the fact that poorly adhered unmelted particles come loose more easily. Despite the insufficient melting of the particles, the HVOF_AT2 coating performed better than the APS-sprayed Al_2O_3 and Al_2O_3-TiO_2 (fused and crushed) coatings. The dense part of the HVOF_AT2 coating's structure appears to compensate the poor coating quality connected to unmelted particles.

Figure 11. Weight losses and standard deviations of the APS and HVOF coatings and bulk Al_2O_3 material after abrasion wear test.

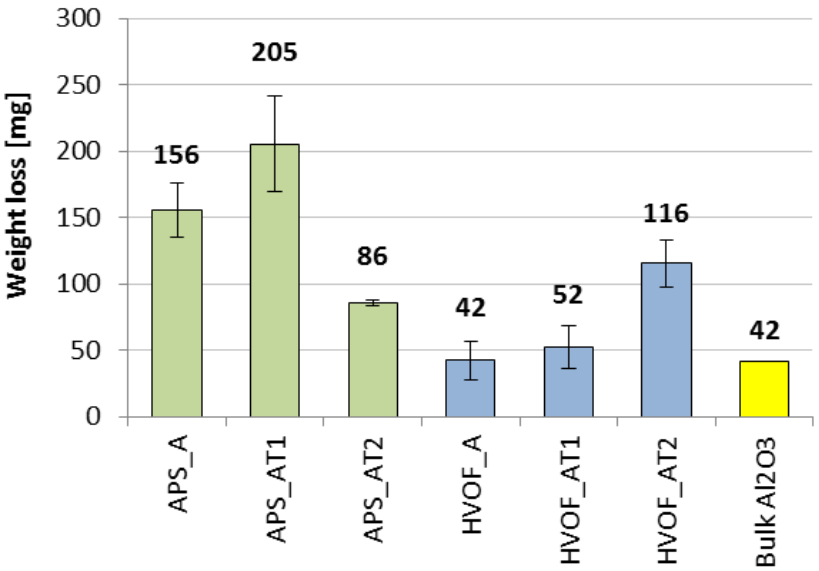

When comparing the coatings sprayed from fused and crushed powders with APS and HVOF spray processes, the Al_2O_3 coatings had better abrasion wear resistance than the coatings with 13% TiO_2 alloying. The TiO_2 addition lowers the hardness and abrasion resistance compared to pure Al_2O_3 [2]. Having a coating structure with varying layers of Al_2O_3 and TiO_2, e.g., coatings designated as APS_AT1 and HVOF_AT1, means that the wear resistance varies between splats of different material.

SEM studies revealed marks of ploughing and plastic deformation of the worn surfaces accompanied with areas of brittle fracture. The mechanism seemed to be the same for all surfaces, with significant

differences only in the amount of brittle fracture areas on the surface arising from the lower ductility and cohesion of the coating, *i.e.*, tendency to brittle fracture. The APS_AT1 coating showed the lowest resistance to abrasive wear and the surface after the abrasion test is presented in Figure 12a. The surface consists of smoother plastically deformed areas and rough valleys showing signs of brittle fracture and unworn splat surfaces, which indicates that pieces of coating have been removed from the top. The wear surface of HVOF_A coating, which had the highest abrasive wear resistance, is shown in Figure 12b. It differs from the higher wear rate surface of APS_AT1 by having larger areas of plastically deformed smooth regions. The areas of brittle fracture seem shallower and smaller in size compared to APS_AT1. According to the abrasion wear results, the ranking of the coatings from highest wear resistance to lowest was HVOF_A, HVOF_AT1, APS_AT2, HVOF_AT2, APS_A, and APS_AT1.

Figure 12. Worn surfaces of (**a**) APS_AT1 and (**b**) HVOF_A coatings after 60-minute abrasion wear test.

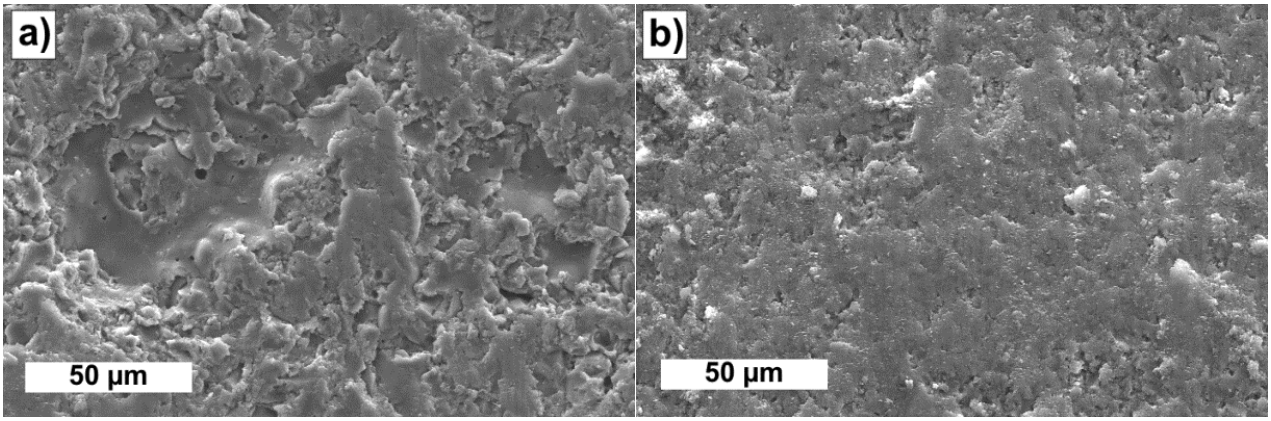

3.5. Erosion Wear Resistance

Figure 13 shows the results (weight losses) from the centrifugal erosion wear tests at 30 ° and 90 ° impact angles. The erosion wear behavior of the coatings was similar to that of the abrasion wear behavior and the ranking of the coatings from best to worse was: HVOF_A, HVOF_AT1, APS_AT2, HVOF_AT2, APS_A, and APS_AT1. The samples fixed to smaller 30 ° impact angle eroded less during the test compared to 90 ° impact angle. Hard and brittle coatings perform well at low impact angles and reach their maximum wear rate at 90 ° angle [38]. The erosion rate of the 30 ° samples ranged between 25% and 50% of the 90 ° impact angle erosion rate.

In addition, in this case, worn surfaces were observed with SEM. The worn surfaces showed that the material is mostly removed by ploughing and brittle fracture at the low impact angles. At 90 ° impact angle, the material is plastically deformed in the impact and removed by brittle fracture. Similar findings were discovered by Westergård [39,40]. Figure 14a shows a single particle impact site on the fine ground surface of the HVOF_AT2 coating. The coating was plastically deformed and some brittle fracture can be seen on the impact mark edges. Parts of the erosive SiO_2 particle have fractured and attached on the impact site. This form of plastic deformation accompanied with minor brittle fracture of the coating is caused by smaller erosive particles with lower kinetic energy. The erosion mechanism with large erosive particles impacting at 90 ° is mostly brittle fracture of the lamellas. Pieces of fractured SiO_2 particles attached on the coating surface were observed at both impact angles. A thin layer of SiO_2,

i.e., tribofilm, was found on several plough-sites, at small impact angles. This can be seen in Figure 14b, where, also, debris from the erosive particle is left on the surface. Material around the wear mark has been removed by brittle fracture caused by particle impacts on the surface.

Figure 13. Weight losses and standard deviations of the APS (green) and HVOF (blue) coatings in the erosion wear test.

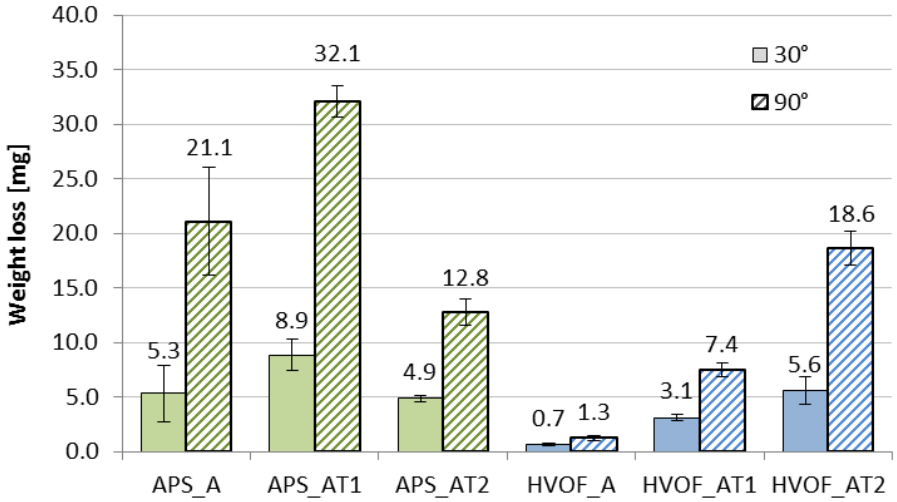

Figure 14. Worn surfaces of (**a**) HVOF_AT2 and (**b**) APS_AT2 coatings after the erosion test.

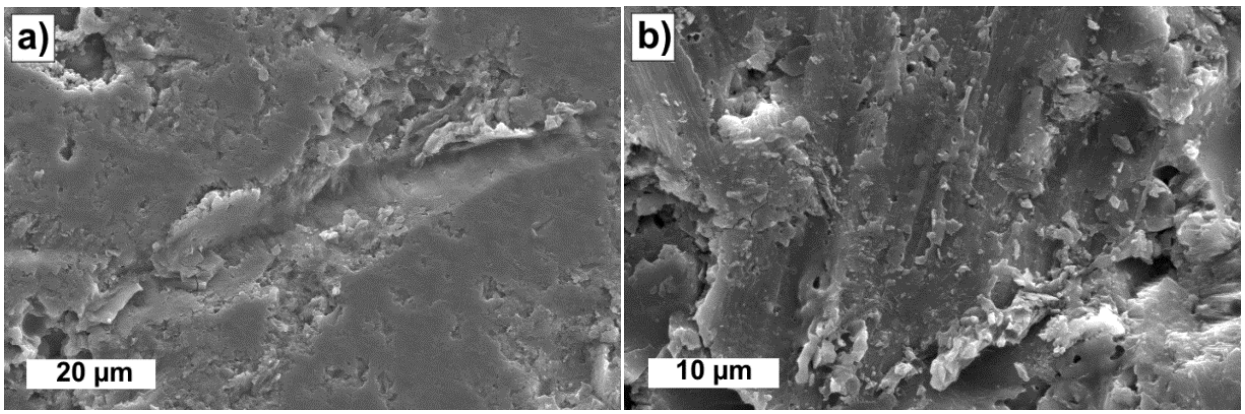

4. Conclusions

Abrasion, erosion, and cavitation erosion wear behavior of APS- and HVOF-sprayed Al_2O_3 and Al_2O_3-TiO_2 coatings sprayed with different powder morphologies were studied and compared. Following conclusions can be made from the results:

- Relatively dense coatings were sprayed from all powders with both spray processes. HVOF-sprayed coatings showed denser structure as higher particle velocities were reached in the process. This resulted in dense structure with small number of horizontal cracks. Larger cracks were observed in plasma-sprayed coatings compared to HVOF coatings.
- HVOF coatings, sprayed from fused and crushed powders, outperformed all other coatings in the wear tests. Higher velocity and small particle size resulted in dense and fine microstructure, which provided the coatings with high wear resistance comparable to bulk Al_2O_3.

- Plasma-sprayed coatings from agglomerated and sintered Al_2O_3-TiO_2 powder showed high wear resistance and outperformed the conventional coatings sprayed with fused and crushed powders. Improved properties were achieved by the agglomeration and sintering powder manufacturing route. This promoted the even distribution of TiO_2 in the coating.
- Coating ranking was basically identical between the abrasion and erosion wear tests as coating wear behavior was very similar. The denser HVOF coatings performed better than their APS counterparts. Improved abrasion and erosion resistance was achieved with the TiO_2 alloying as agglomerated and sintered powder was used. The TiO_2 addition, however, decreased the wear resistance when blended F/C powder was used.
- HVOF-sprayed coatings from F/C powders performed very well compared to other coatings. All the tested coatings showed linear weight loss. Material removal in the cavitation erosion test of the coatings happened purely by brittle fracture revealing the structural differences between the coatings.

Acknowledgments

The authors thank High-Alpha project, funded by industrial partners and the Finnish Funding Agency for Technology and Innovation (Tekes), for financial support of this work. Authors would also like to thank Mikko Kylmälahti of the Tampere University of Technology, Department of Materials Science, for spraying the coatings and Laura Gouillon (summer trainee at the Tampere University of Technology) for helping with the sample preparation and testing.

Conflicts of Interest

The authors declare no conflict of interest.

References

1. Pawlowski, L. *The Science and Engineering of Thermal Spray Coatings*; John Wiley & Sons, Inc.: Oxford, UK, 1995; p. 626.
2. Davis, J.R. *Handbook of Thermal Spray Technology*; ASM International: Materials Park, OH, USA, 2004; p. 338.
3. Bengisu, M. *Engineering Ceramics*; Springer: New York, NY, USA, 2001; p. 620.
4. Gell, M.; Jordan, E.H.; Sohn, Y.H.; Goberman, D.; Shaw, L.; Xiao, T.D. Development and implementation of plasma sprayed nanostructured ceramic coatings. *Surf. Coatings Technol.* **2001**, *146–147*, 48–54.
5. Jordan, E.H.; Gell, M.; Sohn, Y.H.; Goberman, D.; Shaw, L.; Jiang, S.; Wang, M.; Xiao, T.D.; Wang, Y.; Strutt, P. Fabrication and evaluation of plasma sprayed nanostructured alumina-titania coatings with superior properties. *Mater. Sci. Eng. A* **2001**, *301*, 80–89.
6. Varis, T.; Knuuttila, J.; Turunen, E.; Leivo, J.; Silvonen, J.; Oksa, M. Improved protection properties by using nanostructured ceramic powders for HVOF coatings. *J. Therm. Spray Technol.* **2007**, *16*, 524–532.

7. Shaw, L.L.; Goberman, D.; Ren, R.; Gell, M.; Jiang, S.; Wang, Y.; Xiao, T.D.; Strutt, P.R. The dependency of microstructure and properties of nanostructured coatings on plasma spray conditions. *Surf. Coatings Technol.* **2000**, *130*, 1–8.
8. Ahn, J.; Hwang, B.; Song, E.P.; Lee, S.; Kim, N.J. Correlation of microstructure and wear resistance of Al_2O_3-TiO_2 coatings plasma sprayed with nanopowders. *Met. Mater. Trans. A* **2006**, *37*, 1851–1861.
9. Wang, M.; Shaw, L.L. Effects of the powder manufacturing method on microstructure and wear performance of plasma sprayed alumina-titania coatings. *Surf. Coatings Technol.* **2007**, *202*, 34–44.
10. Lima, R.S.; Moreau, C.; Marple, B.R. HVOF-sprayed coatings engineered from mixtures of nanostructured and submicron Al_2O_3-TiO_2 powders: An enhanced wear performance. *J. Therm. Spray Technol.* **2007**, *16*, 866–872.
11. Fauchais, P. Understanding plasma spraying. *J. Phys. D Appl. Phys.* **2004**, *37*, R86–R108.
12. Niemi, K.; Vuoristo, P.; Mäntylä, T. Properties of Alumina Based Coatings Deposited by Plasma and High Velocity Combustion Processes. In Proceedings of 1993 National Thermal Spray Conference, Anaheim, CA, USA, 7–11 June 1993; pp. 469–474.
13. Niemi, K.; Vuoristo, P.; Mäntylä, T. Properties of alumina-based coatings deposited by plasma spray and detonation gun spray processes. *J. Therm. Spray Technol.* **1994**, *3*, 199–203.
14. Niemi, K. Abrasion Wear Characteristics of Thermally Sprayed Alumina Based Coatings. Ph.D. Thesis, Tampere University of Technology, Tampere, Finland, 2009; p. 117.
15. Niemi, K.; Hakalahti, J.; Hyvärinen, L.; Laurila, J.; Vuoristo, P.; Berger, L.-M.; Toma, F.-L.; Shahkhverdova, I. Influence of chromia alloying on the characteristics of APS and HVOF sprayed alumina coatings. In Proceedings of International Thermal Spray Conference 2011, Hamburg, Germany, 27–29 September 2011.
16. Toma, F.-L.; Scheitz, S.; Berger, L.-M.; Sauchuk, V.; Kusnezoff, M.; Thiele, S. Comparative study of electrical properties and characteristics of thermally sprayed alumina and spinel coatings. *J. Therm. Spray Technol.* **2011**, *20*, 195–204.
17. Kreye, H.; Zimmermann, S.; Heinrich, P. The role of the fuel gas in the HVOF process. In *Proceedings of ITSC'95*, Kobe, Japan, 22–26 May 1995; ASM International, Materials Park, OH, USA, 1995; pp. 393–398.
18. Bolelli, G.; Lusvarghi, L.; Manfredini, T.; Mantini, F.P.; Polini, R.; Turunen, E.; Varis, T. Comparison between plasma- and HVOF-sprayed ceramic coatings. Part I: Microstructure and mechanical properties. *Int. J. Surf. Sci. Eng.* **2007**, *1*, 38–61.
19. Vuoristo, P.; Niemi, K.; Matikainen, V.; Hyvärinen, L.; Koivuluoto, H.; Berger, L.-M.; Scheitz, S.; Shakhverdova, I. Structure and Properties of HVOF and Plasma Sprayed Ceramic Alumina-Chromia Coatings Deposited from Fused and Crushed Powders. In *Thermal Spray 2013—Innovative Coating Solutions for the Global Economy*, Proceedings of the ITSC2013 Conference, Busan, Korea, 13–15 May 2013; Lima, R.S., Agarwal, A., Hyland, M.M., Lau, Y.-C., Mauer, G., McDonald, A., Toma, F.-L., Eds.; ASM International: Materials Park, OH, USA, 2013; pp. 465–470.
20. Singh, R.; Tiwari, S.K.; Mishra, S.K. Cavitation erosion in hydraulic turbine components and mitigation by coatings: Current status and future needs. *J. Mater. Eng. Perform.* **2011**, *21*, 1539–1551.

21. Sugiyama, K.; Nakahama, S.; Hattori, S.; Nakano, K. Slurry wear and cavitation erosion of thermal-sprayed cermets. *Wear* **2005**, *258*, 768–775.
22. Yuping, W.; Pinghua, L.; Chenglin, C.; Zehua, W.; Ming, C.; Junhua, H. Cavitation erosion characteristics of a Fe-Cr-Si-B-Mn coating fabricated by high velocity oxy-fuel (HVOF) thermal spray. *Mater. Lett.* **2007**, *61*, 1867–1872.
23. Lima, M.M.; Godoy, C.; Modenesi, P.J.; Avelar-Batista, J.C.; Davison, A.; Matthews, A. Coating fracture toughness determined by vickers identation: An important parameter in cavitation erosion resistance of WC-Co thermally sprayed coatings. *Surf. Coatings Technol.* **2004**, *177–178*, 489–496.
24. Tomlinson, W.J.; Kalitsounakis, N.; Vekinis, G. Cavitation erosion of aluminas. *Ceram. Int.* **1999**, *25*, 331–338.
25. Niebuhr, D. Cavitation erosion behavior of ceramics in aqueous solutions. *Wear* **2007**, *263*, 295–300.
26. Fatjó, G.G.; Hadfield, M.; Vieillard, C.; Sekulic, J. Early stage cavitation erosion within ceramics—An experimental investigation. *Ceram. Int.* **2009**, *35*, 3301–3312.
27. Jafarzadeh, K.; Valefi, Z.; Ghavidel, B. The effect of plasma spray parameters on the cavitation erosion of Al_2O_3-TiO_2 coatings. *Surf. Coatings Technol.* **2010**, *205*, 1850–1855.
28. Schwetzke, R.; Kreye, H. Cavitation Erosion of HVOF Coatings. In *Thermal Spray: Practical Solutions for Engineering Problems*; Berndt, C.C., Ed.; ASM International: Materials Park, OH, USA, 1996; pp. 153–158.
29. Espitia, L.A.; Toro, A. Cavitation resistance, microstructure and surface topography of materials used for hydraulic components. *Tribol. Int.* **2010**, *43*, 2037–2045.
30. *ASTM G32-10 Standard Test Method for Cavitation Erosion Using Vibratory Apparatus*; ASTM International: West Conshohocken, PA, USA, 2010.
31. Kuroda, S.; Dendo, T.; Kitahara, S. Quenching stress in plasma sprayed coatings and its correlation with the deposit microstructure. *J. Therm. Spray Technol.* **1995**, *4*, 75–84.
32. Li, L.; Kharas, B.; Zhang, H.; Sampath, S. Suppression of crystallization during high velocity impact quenching of alumina droplets: Observations and characterization. *Mater. Sci. Eng. A* **2007**, *456*, 35–42.
33. Sakoda, T.; Inaba, M.; Taguchi, K. Microscopic Characteristics and Mechanical Properties of Plasma Sprayed Al_2O_3 Coatings. In *Thermal Spray 2013—Innovative Coating Solutions for the Global Economy*, Proceedings of the ITSC2013 Conference, Busan, Korea; 13–15 May 2013; Lima, R.S., Agarwal, A., Hyland, M.M., Lau, Y.-C., Mauer, G., McDonald, A., Toma, F.-L., Eds.; ASM International: Materials Park, OH, USA, 2013; pp. 406–411.
34. Hurevich, V.; Smurov, I.; Pawlowski, L. Theoretical study of the powder behavior of porous particles in a flame during plasma spraying. *Surf. Coatings Technol.* **2002**, *151–152*, 370–376.
35. Tsochatzidis, N.A.; Guiraud, P.; Wilhelm, A.M.; Delmas, H. Determination of velocity, size and concentration of ultrasonic cavitation bubbles by the phase-Doppler technique. *Chem. Eng. Sci.* **2001**, *56*, 1831–1840.
36. Karimi, A.; Martin, J.L. Cavitation erosion of materials. *Int. Met. Rev.* **1986**, *31*, 1–26.
37. Tucker, R.C. *ASM Handbook Volume 5A: Thermal Spray Technology*; ASM International: Materials Park, OH, USA, 2013.

38. American Society for Metals. *ASM Handbook Volume 18: Friction, Lubrication, and Wear Technology*, 10th ed.; ASM International: Materials Park, OH, USA, 1992.
39. Westergård, R.; Erickson, L.C.; Axén, N.; Hawthorne, H.M.; Hogmark, S. The erosion and abrasion characteristics of alumina coatings plasma sprayed under different spraying coatings. *Tribol. Int.* **1998**, *31*, 271–279.
40. Westergård, R.; Axén, N.; Wiklund, U.; Hogmark, S. An evaluation of plasma sprayed ceramic coatings by erosion, abrasion and bend testing. *Wear* **2000**, *246*, 12–19.